Quaternary Science Reviews 363 (2025) 109439

Contents lists available at ScienceDirect

Quaternary Science Reviews

journal homepage: www.elsevier.com/locate/quascirev

Enhanced East Asian summer monsoon circulation during the Early to Middle Bronze Age

Jiawei Jiang [a], Yancheng Zhang [b,*], Deming Kong [c], Hongxuan Lu [d], Huanye Wang [d], Yu Liang [e], Charlotte Wing Man Lee [a,f], Hongwei Liu [g], Bowen Meng [a,h], Zhouqing Xie [g], Hong Yan [d], Weiguo Liu [d], Zhonghui Liu [a,i,**]

[a] Department of Earth Sciences, The University of Hong Kong, Hong Kong, China
[b] Laoshan Laboratory, Qingdao, 266000, China
[c] College of Ocean and Meteorology, Guangdong Ocean University, Zhanjiang, 524088, China
[d] State Key Laboratory of Loess and Quaternary Geology, Institute of Earth Environment, Center for Excellence in Quaternary Science and Global Change, Chinese Academy of Sciences, Xi'an, 710061, China
[e] School of Earth Resources, China University of Geosciences, Wuhan, 430074, China
[f] Texas A&M University Corpus Christi, Corpus Christi, TX, 78412, United States
[g] Department of Environmental Science and Engineering, Anhui Key Laboratory of Polar Environment and Global Change, University of Science and Technology of China, Hefei, 230026, China
[h] Research Institute of Petroleum Exploration and Development, PetroChina, Beijing, 100083, China
[i] Institute for Climate and Carbon Neutrality, The University of Hong Kong, Hong Kong, China

ARTICLE INFO

Handling Editor: Dr P Rioual

Keywords:
East Asian summer monsoon
Bronze Age
Hydrological change
Biomarker
South China Sea

ABSTRACT

The Holocene East Asian summer monsoon (EASM) evolution has been extensively investigated, yet proxy records show inconsistent variations during the Bronze Age, and spatial patterns of hydroclimatic conditions remain controversial, limiting our understanding of monsoonal behavior and its potential association with culture development. Here we present multiple biomarker records from the northern coast of the South China Sea, which document the strength of monsoon-induced upwelling/mixing effect, to infer Holocene EASM variability. Our multiple biomarker records consistently indicate enhanced EASM circulation during ~6000–9000 cal a BP and ~3300–4500 cal a BP, superimposed on the long-term weakening trend. The enhanced EASM circulation during the Early to Middle Bronze Age challenges the presumed cool/dry climate background and lends support to a tripole pattern of hydroclimatic variability over East China during this period.

1. Introduction

Investigating Holocene East Asian summer monsoon (EASM) variability and hydroclimatic changes in monsoonal region offers crucial insights into our understanding of monsoon dynamics and future climate projections. Direct or indirect EASM records inferred from various archives and proxies generally suggest a long-term Holocene EASM weakening trend (An et al., 2000; Liu et al., 2015; Wang et al., 2005), yet millennial-scale EASM variability and precipitation/hydrological changes over monsoonal regions of East Asia remain controversial (Liu et al., 2015; Zhou et al., 2016). In China and surrounding regions, the Bronze Age (~4000-2200 cal a BP) is characterized by the foundation of the first Chinese dynasty, enhanced cultural exchange between western and eastern Eurasia, and year-round human settlement on the high-altitude northeastern Tibetan Plateau (Chen et al., 2015; Sun et al., 2019; Zhang et al., 2021a). However, several hydrological records from Central East China indicate particularly dry conditions during the Early to Middle Bronze Age (Huang et al., 2018; Xie et al., 2013; Zhang et al., 2021a), while high lake-level/wet conditions and thus increased monsoonal precipitation during this period have been widely documented in lacustrine records from marginal monsoon regions of Northern China (Jiang et al., 2022, 2024; Liu et al., 2015; Zhou et al., 2016). Moreover, stalagmite oxygen isotopic records from East Asia (Dykoski et al., 2005; Wang et al., 2005; Yang et al., 2019), interpreted as EASM

* Corresponding author.
** Corresponding author. Department of Earth Sciences, The University of Hong Kong, Hong Kong, China.
E-mail addresses: zhangpaleo@gmail.com (Y. Zhang), zhliu@hku.hk (Z. Liu).

https://doi.org/10.1016/j.quascirev.2025.109439
Received 16 February 2025; Received in revised form 12 May 2025; Accepted 19 May 2025
Available online 26 May 2025

strength or source water isotopic signal indicators (Dykoski et al., 2005; Zhang et al., 2018), exhibit inconsistent variations during the Bronze Age (Cai et al., 2021; Dykoski et al., 2005; Wang et al., 2005; Zhang et al., 2021a). Hence, the climate background during the Bronze Age and its association with cultural development have been much disputed (Xie et al., 2013; Yu et al., 2020; Zhang et al., 2021a). The presumed cool/dry conditions in East Asia during the Bronze Age (Chen et al., 2015; Sun et al., 2019) seem to follow the conventionally recognized climatic conditions of the "4.2 ka event" (deMenocal, 2001; Railsback et al., 2018), a well-studied abrupt climatic event at ~4200 cal a BP that lasted for ~200 years (deMenocal, 2001; Railsback et al., 2018). However, recent studies propose that climatic expressions of the "4.2 ka event" appear to be regionally diverse (Lin et al., 2022; Railsback et al., 2018) and may not be as remarkable as generally assumed (Mckay et al., 2024).

The spatial patterns of hydroclimatic conditions in East Asia across different climatic periods have been extensively studied (Cao et al., 2024; Chiang et al., 2017; Jiang et al., 2021; Liu et al., 2014; Xu et al., 2024; Zhang et al., 2018). The meridional tripole pattern of monsoonal precipitation, suggesting wet conditions over Northeastern and Southeastern China corresponding to dry conditions over Central East China at interannual timescale, has been proposed (Chiang et al., 2017), and recent studies also suggest a tripole pattern of monsoonal precipitation in East Asia during the Last Glacial Termination (Zhang et al., 2018) and over the last millennium (Jiang et al., 2021; Xu et al., 2024). However, model simulations and pollen records show a north-south dipole pattern of Holocene precipitation/hydroclimatic changes in East Asia (Li et al., 2024; Liu et al., 2014; Xu et al., 2024). The spatial patterns of hydroclimatic conditions over this region during the Bronze Age remain poorly examined, largely due to limited records from Southeastern China and uncertainties in hydrological records from such a humid region. Biomarker records from the Chinese Marginal Seas provide critical insights into EASM variations (Jiang et al., 2025; Lee et al., 2019; Wang et al., 2021), which are particularly valuable for filling spatial gaps in monsoonal records from Southeastern China and clarifying EASM variability during the Bronze Age, with important implication in deciphering spatial pattern of hydroclimatic conditions in East Asia and understanding its influences on human-environment interactions.

Here we present high-resolution Holocene alkenone and glycerol dialkyl glycerol tetraether (GDGT) records from core HKGS-A (22°09′09″N, 114°26′55″E) that can be linked to the strength of coastal upwelling/mixing at the northern coast of the South China Sea (SCS) (Figs. 1 and 2, S1, Supplementary Data). Sea surface temperature (SST) in certain upwelling regions along the northern continental margin of the SCS is noticeably influenced by cooling effects associated with monsoon-induced coastal upwelling (Fig. 1). Previous studies (Lee et al., 2019; Wang et al., 2021) have suggested that when SST changes in upwelling regions are inconsistent with global/open ocean SST, SST and vertical thermal gradient can largely document the strength of

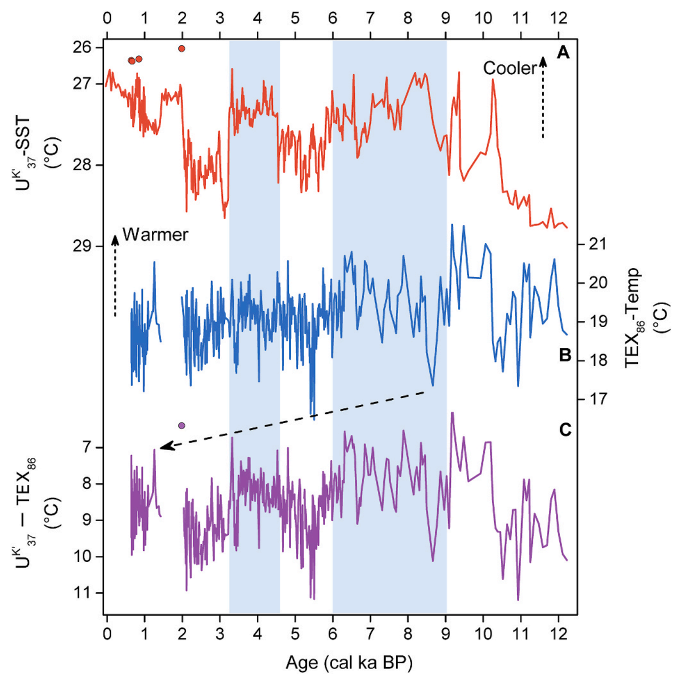

Fig. 2. Holocene biomarker records from core HKGS-A. (A) $U^{K'}_{37}$-SST, (B) TEX_{86}-based subsurface temperature, (C) vertical thermal gradient ($U^{K'}_{37}-TEX_{86}$). Blue bars highlight the time intervals with strengthened summer upwelling at the northern coast of the SCS and thus enhanced EASM strength.

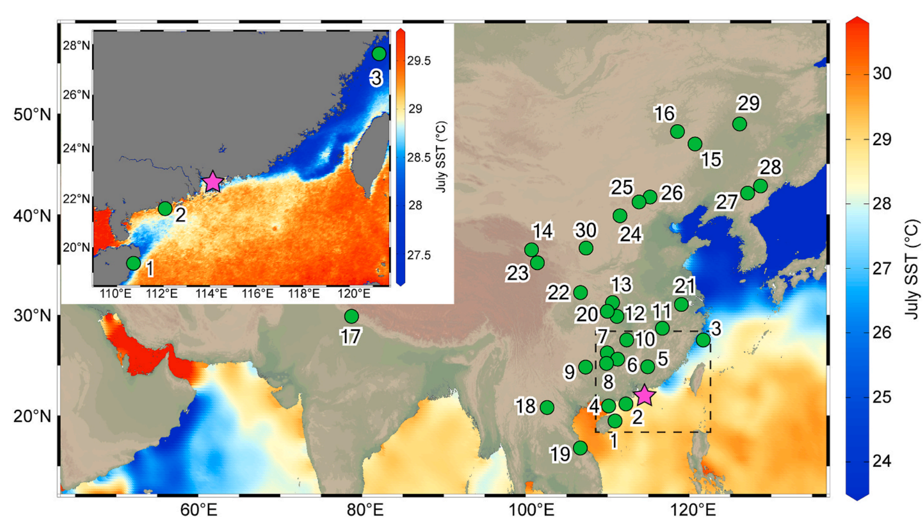

Fig. 1. Site location map. Locations of core HKGS-A (pink star) and other records discussed in the main text (green dots). Site 1: Qionghai, 2: YJ, 3: MD06-3040, 4: Huguangyan Maar Lake, 5: Dahu Swamp, 6: Shiwangutian Peatland, 7: Daping Swamp, 8: Dapingtang Swamp, 9: Dongge Cave, 10: Jiulong Cave, 11: Shennong Cave, 12: Heshang Cave, 13: Dajiuhu Peatland, 14: Lake Qinghai, 15: Lake Moon, 16: Lake Yihesariwusu, 17: Sahiya Cave, 18: Tham Doun Mai Cave, 19: Thien Duong Cave. Sites 20–30 listed in Table S1. Basemap shows July mean SST for 1955–2017 AD from World Ocean Atlas (2018) (Locarnini et al., 2018). The inset shows high-resolution July mean SST for 1985–2006 AD from the AVHRR data set (Casey et al., 2013), which indicates our site located at summer-upwelling region at the northern coast of the SCS.

monsoon-induced upwelling/mixing effect and thus EASM variability. Our multiple biomarker records documenting Holocene EASM variability, together with existing terrestrial and marine records, enable the assessment of EASM behavior and spatial patterns of hydroclimatic variability over East Asia during the Bronze Age.

2. Materials and methods

2.1. Materials and chronology

A 60.2-m-long gravity core HKGS-A (22°09′09″N, 114°26′55″E) was retrieved from the southeastern waters off Hong Kong at ~30 m water depth through a Hong Kong Geological Survey Project (Fig. 1). This site displays prominent seasonal variations in sea surface salinity (SSS, ~29.5 psμ in June-July-August, JJA, and ~32.5 psμ in December-January-February, DJF, Lee et al., 2019; Zweng et al., 2019) and SST (~27.5 °C in JJA and ~18.5 °C in DJF, Casey et al., 2013; Lee et al., 2019). Summer SSS variations at this site are influenced by the Pearl River discharge, while freshwater discharge does not show evident impact on SST changes (Lee et al., 2019). Summer SST along the northern SCS coasts reveal that our site experiences noticeable cooling effects of ~1 °C, which is linked to the monsoon-induced upwelling (Fig. 1, Lee et al., 2019; Zweng et al., 2019). Lithological (Fig. S1A, Fyfe et al., 1999) and seismic profiles suggest that the upper ~15 m of this core is composed of continuously deposited soft sediments containing bioturbation and shells, roughly covering the Holocene (Davis, 1999; Fyfe et al., 1999). The $U^{K'}_{37}$-SST record from the upper ~3 m of this core, which presents high-resolution monsoon-induced upwelling variations in the northern SCS coast over the last two millennia, has been reported previously (Lee et al., 2019).

The chronology of the upper ~15 m of core HKGS-A was established using twelve ^{14}C dates, including seven reported previously (Lee et al., 2019) and five additional dates (Fig. S1B, Supplementary Data). We prepared samples of complete shells (or their fragments) for ^{14}C dating at Beta Analytic Inc., USA. These age control points were then operated within the R script-based BACON software (Blaauw and Christen, 2011) through default parameters. The software incorporated the Marine20 calibration curve, incorporating a 50-year correction for regional reservoir age based on the nearest sites in the Marine20 database (Heaton et al., 2020). The core chronology suggests an age of ~12,300 cal a BP at the depth of ~15 m (Fig. S1B, Supplementary Data).

The upper ~15 m of core HKGS-A was sampled at intervals of ~2–10 cm for biomarker analysis. Based on the core chronology (Fig. S1B, Supplementary Data), this sampling approach that yielded ~450 samples, provides a high temporal resolution of ~10–50 years throughout the Holocene. The alkenone results for the upper ~3 m have been reported by Lee et al. (2019), and here we analyzed alkenones in the remaining samples and GDGTs in all samples.

2.2. Biomarker analysis

Freeze-dried samples were extracted ultrasonically (3 × 30 min) with solvent of dichloromethane: methanol (9:1, v/v, 15 ml each time). The total lipids were dried under N_2 and saponified with 6 % KOH in MeOH for at least 12 h at room temperature. Subsequently, 1.5 ml of NaCl in water (5 %, w/w) was added, and the neutral solution was extracted with 4 ml *n*-hexane. The neutral solution was then separated into three fractions with silica gel column chromatography using 4 ml *n*-hexane, 4 ml dichloromethane, and 4 ml methanol, respectively, while the dichloromethane fraction contains alkenones and the methanol fraction contains GDGTs.

The alkenone fraction was analyzed on an Agilent 7890 Gas Chromatography (Agilent DB-1 column: 60 m × 250 μm × 0.10 μm film thickness) with Flame Ionization Detection (FID) at The University of Hong Kong, using *n*-C_{36} *n*-alkane as internal standard for quantification. Each sample was injected in a splitless mode, with H_2 as carrier gas. The oven temperature program for alkenone analysis was: 60 °C (1 min) to 270 °C at 13 °C/min, and then to 310 °C at 3 °C/min (held 30 min). The laboratory standards were repeatedly analyzed to assess the analytical precision. The $U^{K'}_{37}$ index was calculated according to the equation by Prahl et al. (1988) and converted to SST values based on the SCS regional calibration (Pelejero and Grimalt, 1997):

$$U^{K'}_{37} = C_{37:2} \ / \ (C_{37:2} + C_{37:3}) \quad (1)$$

$$SST = (U^{K'}_{37} - 0.092) \ / \ 0.031 \quad (2)$$

where $C_{37:2}$ and $C_{37:3}$ are concentrations of di- and tri-unsaturated C_{37} alkenones, respectively. Different alkenone calibration equations (Tierney and Tingley, 2018; Pelejero and Grimalt, 1997) would yield the same pattern of SST changes, which is also true for the TEX_{86} proxy (Schouten et al., 2002). Analytical uncertainties in our lab were typically less than 0.005 unit for $U^{K'}_{37}$ (equivalent to ~0.2 °C for SST estimate) and 5 % for the C_{37} concentration.

The GDGTs fraction was analyzed on a Shimadzu LC-MS 8030 high-performance liquid chromatography with atmospheric pressure chemical ionization–mass spectrometry in Xi'an at the Institute of Earth Environment, Chinese Academy of Sciences. Briefly, the methanol fraction was dried under N_2, re-dissolved in n-hexane/isopropanol (99:1; v/v) and filtered through a 0.22 μm polytetrafluoroethylene filter after adding a known amount of C_{46} internal standard. Separation of GDGTs was achieved with an Inertsil CN-3 column (250 mm × 4.6 mm, 3 μm; GL Sciences Inc.) at 40 °C using *n*-hexane/isopropanol (9:1, v/v) and *n*-hexane as elutes for pump A and pump B, respectively. Mass spectrometry scanning was performed in selected ion monitoring mode that targeted specific $[M + H]^+$ ions (isoprenoid GDGTs: caldarchaeol/GDGT-0, 1302.3; GDGT-1, 1300.3; GDGT-2, 1298.3; GDGT-3, 1296.3; cren, 1292.3; crenarchaeol′ (cren′), 1292.3). The TEX_{86} (tetraether index of 86 carbon atoms, Schouten et al., 2002) and TEX_{86}-based temperature (Kim et al., 2010) are calculated as follows:

$$TEX_{86} = (GDGT\text{-}2 + GDGT\text{-}3 + cren') \ / \ (GDGT\text{-}1 + GDGT\text{-}2 + GDGT\text{-}3 + cren') \quad (3)$$

$$SST = 68.4 \times \log(TEX_{86}) + 38.6 \quad (4)$$

Analytical uncertainties for our laboratory standards are typically less than 0.01 unit for TEX_{86}. The breaks of TEX_{86}-based temperature record at the top ~0.6 m and ~2.6–3.0 m depth (Fig. 2B, Supplementary Data), due to missing GDGT fractions, roughly corresponding to the past ~700 years and the time interval of ~1500–2000 cal a BP, respectively, do not affect the overall variation pattern of the record.

3. Results

The $U^{K'}_{37}$-SST record does not appear to show discernible long-term trend over the investigated period, with low values occurring at the time intervals of ~6000–9000 cal a BP, ~3300–4500 cal a BP, ~1500–2000 cal a BP, and ~600–1100 cal a BP (Fig. 2A). The TEX_{86}-based temperature record displays a long-term Holocene cooling trend, with relatively high values observed at low $U^{K'}_{37}$-SST intervals (Fig. 2A and B). Two samples show anomalously low TEX_{86} (Supplementary Data), indicating substantial non-Thaumarchaeota contribution in marine settings (Wang et al., 2023a) that could confound the TEX_{86}-temperature estimation, and therefore, were excluded from TEX_{86}-based temperature record (Fig. 2B). The difference between $U^{K'}_{37}$- and TEX_{86}--based temperatures ($U^{K'}_{37}-$ TEX_{86}) show relatively low values during 6000–9000 cal a BP and ~3300–4500 cal a BP (Fig. 2C), superimposed on a long-term increasing trend. The two intervals, with lower $U^{K'}_{37}$-SST values at the site, generally correspond to the Holocene Climatic Optimum and the Early to Middle Bronze Age, respectively. Alkenone C_{37}

content shows an increasing trend during the early to mid-Holocene, with high values occurring at the time interval of ~3000–4500 cal a BP (Supplementary Data).

4. Discussion

4.1. Proxy interpretation

The $U^{K'}_{37}$-SST signal intrinsically records both winter and summer imprints, with interpretation of this index depending on the specific oceanographic settings (Kong et al., 2014, 2015; Lee et al., 2019; Wang et al., 2021; Zhang et al., 2019, 2021b). The $U^{K'}_{37}$-SST value for core-top sample in HKGS-A is higher than modern annual mean SST but close to summer SST (Supplementary Data, Casey et al., 2013; Lee et al., 2019). This is consistent with surface sediment calibration from the coastal regions of the Chinese Marginal Seas (Wang et al., 2023b) and existing cores from the northern SCS coast (Kong et al., 2015), which seems to be associated with high-nutrient conditions (Wang et al., 2023b). The $U^{K'}_{37}$-SST record from core HKGS-A does not display a discernible long-term trend during the Holocene (Fig. 2A), and is inconsistent with existing $U^{K'}_{37}$-SST records from the northern SCS interpreted as winter imprints (Kong et al., 2014; Zhang et al., 2019) and synthesized tropical SST record (Marcott et al., 2013). Previously reported $U^{K'}_{37}$-SST records from upwelling regions of the northern SCS coast are also inconsistent/inverse with global/tropical SST variations (Kong et al., 2015; Lee et al., 2019; Wang et al., 2021). This cannot be explained by the winter imprint, as cooler winters generally occur under cooler climatic conditions. Cooling induced by summer coastal upwelling appears to be the (only) plausible explanation for our SST signal, which must have substantially altered the global temperature background and winter imprint (Lee et al., 2019; Wang et al., 2021). Therefore, decreased local SST effectively reflects enhanced summer upwelling at the northern SCS coast that could be linked to enhanced EASM strength.

Recent studies suggest that TEX_{86} values tend to represent temperature of subsurface water rather than surface water over the western Pacific marginal sea (Xing et al., 2015) and the northern coast of the SCS (Wang et al., 2021; Zhang et al., 2021c). Considering the inverse variations between paired TEX_{86}-based temperature and onsite $U^{K'}_{37}$-SST (Fig. 2A and B), we here also interpret the TEX_{86} thermometer as an indicator of integrated water column temperature biased toward subsurface (Wang et al., 2021; Zhang et al., 2021c). Hence, $U^{K'}_{37} - TEX_{86}$ could largely represent the vertical thermal gradient without the impact of chronological uncertainty. The $U^{K'}_{37} - TEX_{86}$ record displays a long-term increasing trend with low values occurring at the SST cooling intervals (Fig. 2A–C), indicating enhanced upwelling substantially alters the original SST signal and thus reduced vertical thermal gradient.

The inconsistency between $U^{K'}_{37}$-SST and tropical/open ocean SST, together with reversed $U^{K'}_{37}$-SST and onsite TEX_{86}-based temperature variations, strongly suggest the monsoon-induced upwelling effects at our site, thereby enabling the inference of Holocene EASM variability.

4.2. Holocene summer upwelling and EASM variability

Decreased $U^{K'}_{37}$-SST that contrasts with increased onsite TEX_{86}-based subsurface temperature, indicate enhanced summer upwelling in the northern coast of the SCS and thus strengthened EASM, and vice versa. The increased vertical thermal gradient towards the late Holocene (Fig. 2C) suggest a long-term Holocene EASM weakening trend following the decreased summer insolation (Laskar et al., 2004), consistent with existing EASM records (Dykoski et al., 2005; Liu et al., 2015; Wang et al., 2005). Notably, $U^{K'}_{37}$-SST indicate substantially enhanced EASM strength during ~6000–9000 cal a BP and ~3300–4500 cal a BP, superimposed on the long-term weakening trend (Fig. 2A–C). Enhanced EASM strength during the early Holocene has been well documented in various terrestrial records (Liu et al., 2015; Wang et al., 2005), while the EASM behavior during ~3300–4500 cal a BP is less well addressed. Terrestrial anthropogenic impacts were relatively limited in southeastern China before ~2000–3000 cal a BP (Ma et al., 2020), with minimum anthropogenic perturbations on coastal environment. Hence, high alkenone C_{37} content during ~3300–4500 cal a BP (Supplementary Data) might be associated with more upwelling-induced subsurface nutrients (Lee et al., 2019; Wang et al., 2021), again indicating enhanced EASM strength. Notably, $\delta^{18}O$ records from South Asia show relatively negative values, also indicating enhanced monsoon circulation, during ~3300–4500 cal a BP (Fig. 3C, Gupta et al., 2024; Kathayat et al., 2017), while several Chinese stalagmite $\delta^{18}O$ records do not suggest particularly enhanced EASM during this period (Fig. 3D–Wang et al., 2005; Yang et al., 2019). The weak expression of substantially enhanced EASM strength in Chinese stalagmite $\delta^{18}O$ records during this period remains enigmatic.

4.3. Enhanced EASM during the early to middle Bronze age

Holocene millennial-scale climatic fluctuations are suggested to be linked to solar activities (Bond et al., 2001; Wang et al., 2005). No particular changes in greenhouse gas and volcanic forcings were observed during ~3300–4500 cal a BP, while solar activity remained high (Fig. 3A, Steinhilber et al., 2012). Substantially enhanced EASM strength during ~3300–4500 cal a BP, corresponds to the Early to Middle Bronze Age, could be inferred from SST gradient variations and other marine records from the Chinese marginal seas (Fig. 4C–E). The $U^{K'}_{37}$-SST gradient between HKGS-A and YJ, a site located at the northern coast of the SCS but experienced limited upwelling effects (Fig. 1, Zhang

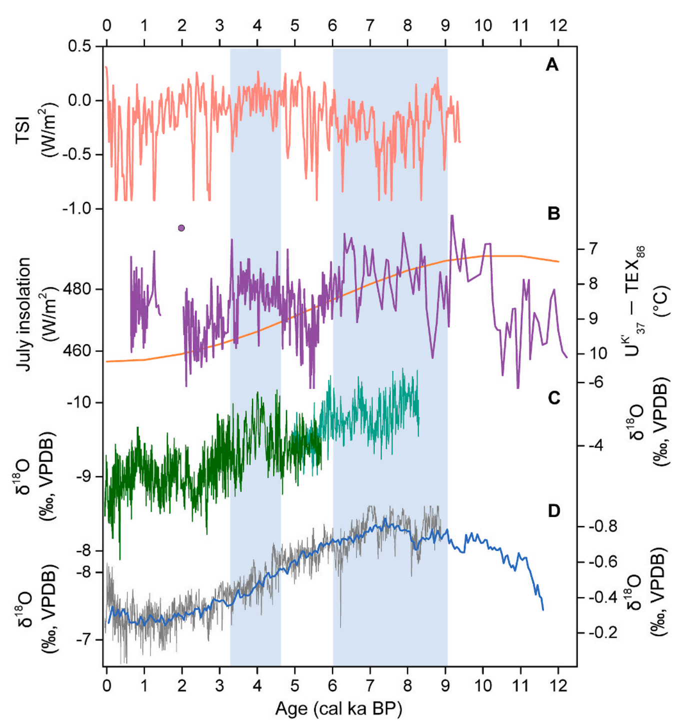

Fig. 3. Holocene climatic records and forcings. (A) Total solar irradiance (TSI, Steinhilber et al., 2012), (B) $U^{K'}_{37} - TEX_{86}$ (purple line, this study) and mean July insolation at 20°N (orange line, Laskar et al., 2004), (C) $\delta^{18}O$ record from Sahiya and Mahadev Cave (dark and light blue line, respectively, Gupta et al., 2024; Kathayat et al., 2017), (D) $\delta^{18}O$ record from Dongge Cave (grey line, Wang et al., 2005) and synthesized speleothem $\delta^{18}O$ record from monsoonal China (blue line, Yang et al., 2019). Blue bars highlight the time intervals with strengthened summer upwelling at the northern coast of the SCS and thus enhanced EASM strength.

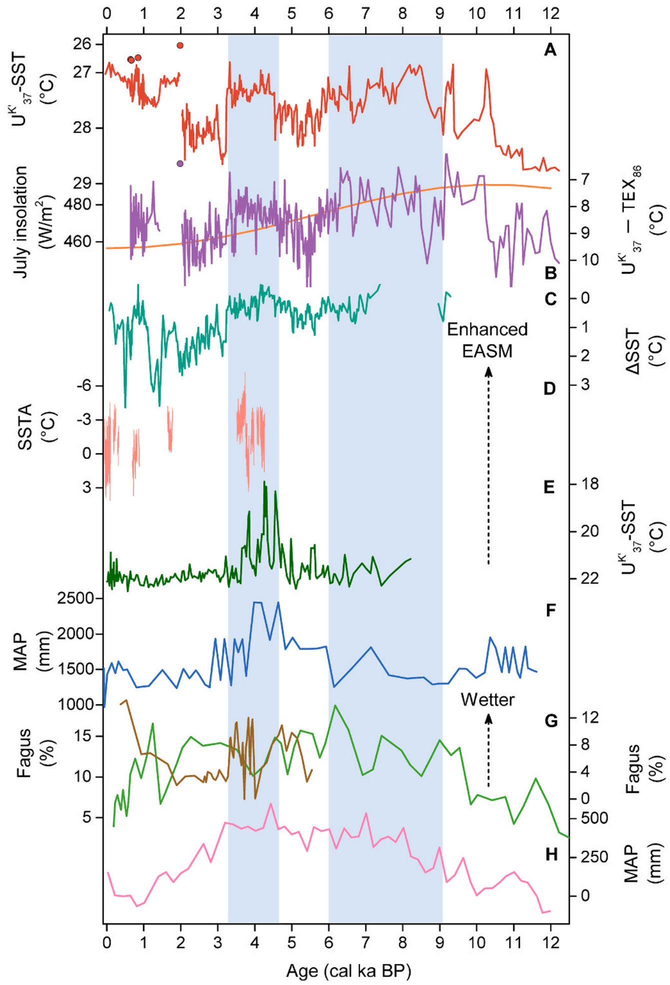

Fig. 4. Holocene climatic records from the Chinese marginal seas and Southeastern China. (A) $U^{K'}_{37}$-SST (this study), (B) $U^{K'}_{37}-TEX_{86}$ (purple line, this study) and mean July insolation at 20°N (orange line, Laskar et al., 2004), (C) $U^{K'}_{37}$-SST gradient between HKGS-A and YJ (Zhang et al., 2019), HKGS-A minus YJ, ΔSST, (D) coral Sr/Ca-based SST anomaly records from Qionghai (Chen et al., 2023), (E) $U^{K'}_{37}$-SST record from core MD06-3040 (Kajita et al., 2018), (F) Pollen-based mean annual precipitation (MAP) record from Shiwangutian peatland (Zhao et al., 2024), (G) *Fagus* percentage records from Daping Swamp and Dapingtang Peatland (green and brown line, respectively, Li et al., 2019; Zhong et al., 2015), (H) pollen-based synthesis of mean annual precipitation in South China (Li et al., 2024). Blue bars highlight the time intervals with strengthened summer upwelling at the northern coast of the SCS and thus enhanced EASM strength.

et al., 2019), could effectively reflect the monsoon-induced upwelling variability while eliminating the influence of environmental temperature background (Fig. 4C). Relatively low SST gradient during SST colling intervals at HKGS-A (Fig. 4A–C) suggests a substantial upwelling control on SST at HKGS-A that exceeds the environmental temperature changes. The overall increase in SST gradient since ~3000 cal a BP reverses the SST cooling trend (Fig. 4A–C), largely reflecting upwelling changes within the late Holocene cooling context and highlighting the substantially enhanced EASM strength during the Early to Middle Bronze Age. Additionally, coral-based SST records from Qionghai, also located at an upwelling region of the northern SCS coast (Fig. 1), show relatively low SST during ~3500–4000 cal a BP (Fig. 4D–Chen et al., 2023) and thus enhanced EASM strength. The $U^{K'}_{37}$-SST record from the upwelling region of the East China Sea coast (Fig. 1) displays low values during ~3500–4500 cal a BP (Fig. 4E–Kajita et al., 2018), while such cooling signals have not been observed in open oceans (Zhang et al., 2021b). This indicates enhanced upwelling in the East China Sea coast was also linked to enhanced EASM strength during the Early to Middle Bronze Age.

Modern observations, proxy reconstructions, and model simulations collectively suggest that precipitation changes in Northeastern and Southeastern China appear to be positively linked to EASM strength (Chiang et al., 2017; Ding et al., 2008; Liu et al., 2014). Here we summarize terrestrial precipitation/hydrological records from these regions to infer EASM behavior during the Early to Middle Bronze Age (Figs. 4 and 5A–F). Alkenone %$C_{37:4}$ and pollen records from marginal monsoon regions of Northern China (Fig. 5A–C, Jiang et al., 2022; Jiang et al., 2024; Wu et al., 2019) suggest high lake-level/wet conditions during the Early to Middle Bronze Age. Moreover, an increased frequency of Yellow River flooding during the Early to Middle Bronze Age has been reported (Yu et al., 2020), indicating excessive precipitation and overall wet

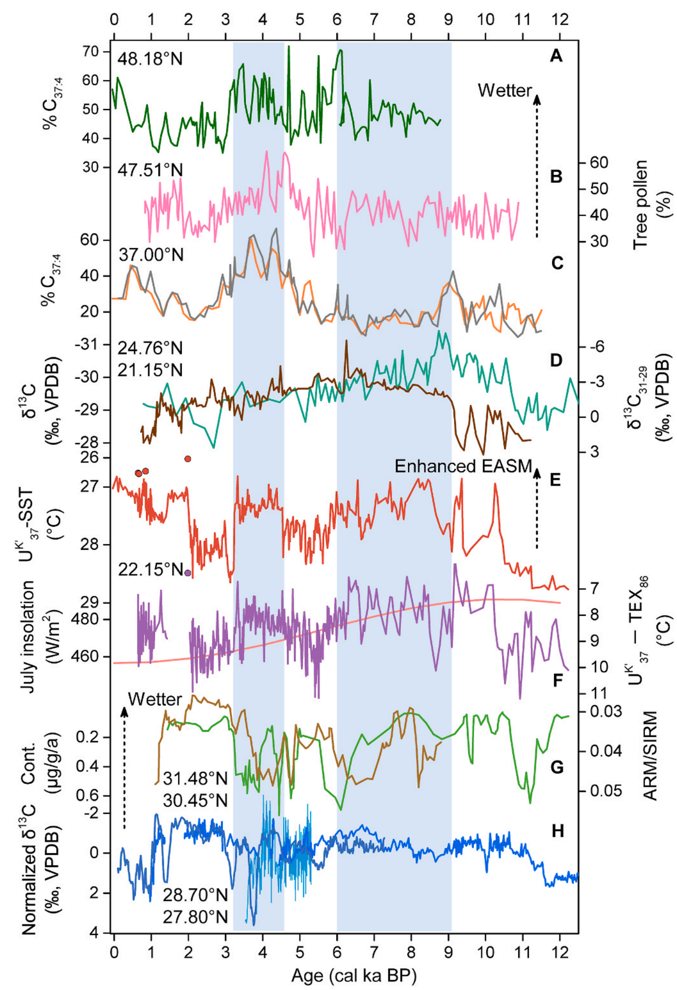

Fig. 5. EASM records from core HKGS-A and terrestrial hydrological records from East Asia. (A) Alkenone %$C_{37:4}$ record from Lake Yihesariwusu (Jiang et al., 2024), (B) tree pollen percentage record from Lake Moon (Wu et al., 2019), (C) alkenone %$C_{37:4}$ records from Lake Qinghai (Jiang et al., 2022), (D) $\delta^{13}C_{org}$ record from Dahu Swamp and *n*-alkane $\delta^{13}C_{31\text{-}29}$ record from Huguangyan Maar Lake (green and brown line, respectively, Jia et al., 2015; Zhong et al., 2010), (E) $U^{K'}_{37}$-SST from core HKGS-A (this study), (F) $U^{K'}_{37}-TEX_{86}$ from core HKGS-A (purple line, this study), and mean July insolation at 20°N (orange line, Laskar et al., 2004), (G) environmental magnetism parameter ARM/SIRM record from Heshang Cave and mass accumulation rate of aerobic hopanoids in Dajiuhu peatland (brown and green line, respectively, Xie et al., 2013), (H) normalized speleothem $\delta^{13}C$ records from Shennong and Jiulong caves (Zhang et al., 2021a). Blue bars highlight the time intervals with strengthened summer upwelling at the northern coast of the SCS and thus enhanced EASM strength.

conditions. Meanwhile, carbon isotopic records from Southeastern China (Fig. 5D–Jia et al., 2015; Zhong et al., 2010) indicate wet conditions during the Early to Middle Bronze Age and long-term Holocene drying trends. Several pollen records from this region also suggest wet conditions during the Early to Middle Bronze Age (Fig. 4F–H, Li et al., 2024; Li et al., 2019; Zhao et al., 2024; Zhong et al., 2015). Hence, terrestrial hydrological records from Northeastern and Southeastern China strongly support substantially enhanced EASM strength during the Early to Middle Bronze Age.

Terrestrial hydrological records from Southeastern China show wet conditions during ~6000–9000 cal a BP (Fig. 5D–Jia et al., 2015; Zhong et al., 2010), indicating enhanced EASM strength as inferred from marine records (Fig. 5A–D). However, hydroclimatic conditions in some regions of Northern China could have been influenced by the inland high-pressure system associated with atmospheric changes during the early to mid-Holocene (Jiang et al., 2024), and the low lake-level/dry conditions during ~6000–9000 cal a BP (Fig. 5A–C, Jiang et al., 2022; Jiang et al., 2024; Wu et al., 2019) appear to reflect such atmospheric control rather than monsoonal precipitation changes.

4.4. Spatial patterns of hydroclimatic variability

Marine and terrestrial records collectively suggest substantially enhanced EASM strength during the Early to Middle Bronze Age (Figs. 4 and 5A-F). We further summarize terrestrial hydrological records to infer spatial patterns of hydroclimatic variability over East Asia during this period (Fig. 6, Table S1). Wet conditions during the Early to Middle Bronze Age have been widely documented in lacustrine, peat, and paleosol records from Northeastern and Southeastern China (Fig. 5A–D, 6, Table S1, Cheng et al., 2013; Hong et al., 2005; Jia et al., 2015; Jiang et al., 2006; Jiang et al., 2022; Jiang et al., 2024; Li et al., 2019; Li and Liu, 2018; Stebich et al., 2015; Wang et al., 2014; Wu et al., 2019; Xiao et al., 2004; Zhao et al., 2024; Zhong et al., 2010; Zhong et al., 2015; Zhou et al., 2016), while hydrological records inferred from various proxies and archives in Central East China generally indicate dry conditions (Fig. 5G, H, 6, Table, S1, Huang et al., 2018; Lu et al., 2019; Tan et al., 2018; Xie et al., 2013; Zhang et al., 2021a; Zhao et al., 2016). The contrasting hydrological variations in Northeastern/Southeastern China and Central East China, together with substantially enhanced EASM strength supported by marine records from the Chinese marginal seas, during the Early to Middle Bronze Age, support the meridional tripole pattern of hydroclimatic variability over East China during this period. The tripole pattern of hydroclimatic variability during the Early to Middle Bronze Age observed from climatic records (Figs. 5 and 6) is inconsistent with the simulated millennial-scale hydrological variability, which tends to show a dipole pattern in East China (Fig. 3 in Zhang et al., 2018), and the north-south dipole pattern of Holocene precipitation/hydrological changes suggested by model and pollen results (Li et al., 2024; Liu et al., 2014). Wet conditions in Southeastern China and dry conditions in Central East China during ~6000–9000 cal a BP (Fig. 5G–G, H) are consistent with the contrasting hydroclimatic changes during the Early to Middle Bronze Age. However, the hydroclimatic variability over East Asia during ~6000–9000 cal a BP does not follow the tripole pattern observed during the Early to Middle Bronze Age, which appears to be associated with atmospheric control on early to mid-Holocene drought in Northeastern China (Fig. 5A–C).

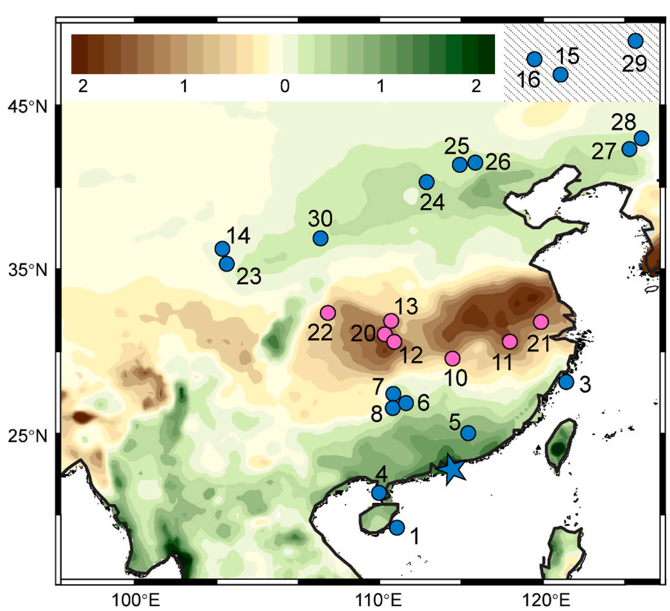

Fig. 6. Tripole pattern of hydroclimatic variability over East China during the Early to Middle Bronze Age. Star represents site HKGS-A from this study, dots and dashed square represent sites from previous studies. The blue color indicates wet conditions/enhanced ESAM strength during the Early to Middle Bronze Age, the pink color indicates dry conditions during this period. Records and references are listed in Table S1, numbers refer to site locations in Fig. 1 and Table S1. Basemap showing tripole pattern of modern interannual variability of precipitation over East Asia (Zhang et al., 2018. No data available above 45°N, marked with shading), green and yellow colors indicate wet and dry conditions, respectively.

Previous studies hypothesized that the climate background during the Early to Middle Bronze Age have been notably influenced by a severe cool/dry event that occurred at ~4200 cal a BP (Blanco-González et al., 2018; Sun et al., 2019), while recent data integrations suggest that climatic expressions of the “4.2 ka BP event” appear to be regionally diverse (Lin et al., 2022; Railsback et al., 2018). Substantially enhanced EASM strength and thus overall wet conditions in Northeastern and Southeastern China challenge the presumed cool/dry conditions over East China during the Early to Middle Bronze Age (Chen et al., 2015; Sun et al., 2019). In the context of contrasting hydrological variations in Northeastern and Central East China, the northeastward migration of archaeological sites in East China (Hosner et al., 2016), the final demise of the Neolithic cultures in the lower Yangtze region (Zhang et al., 2021a), and higher frequency of floods in the middle to lower Yellow River region (Yu et al., 2020) over the Early to Middle Bronze Age appear to be corroborated by a plausible climatic explanation.

Controlling mechanisms of the tripole pattern of hydroclimatic variability in monsoonal East Asia across different timescales are much disputed (Huang et al., 2023; Jiang et al., 2021; Xu et al., 2024; Zhang et al., 2018). Wet conditions observed in Northeastern and Southeastern China and thus increased monsoonal precipitation during the Early to Middle Bronze Age appear to be associated with enhanced EASM strength. However, dry conditions in Central East China under an enhanced EASM background may suggest the dominant control of Western Pacific Subtropical High (WPSH) or westerlies dynamics on regional hydrological variability. Recent studies attribute dry conditions in Central East China over the last millennium primarily to the westward extension of the WPSH (Xu et al., 2024). Yet, this mechanism does not adequately reconcile with decreased SST signal observed in the upwelling region of the East China Sea during the Early to Middle Bronze Age (Kajita et al., 2018), which indicates enhanced coastal upwelling mechanistically linked to EASM intensification. Alternatively, the northward displacement of westerlies, suggested by model simulations and reconstructions (Chiang et al., 2017; Zhang et al., 2018), may induce drier conditions in Central East China and thus a tripole pattern of hydroclimatic variability. Additionally, recent studies reveal exceptional warm conditions in northwestern China during the Early to Middle Bronze Age (Jiang et al., 2022; Xiang et al., 2024). Combined with our evidence of enhanced EASM strength, further investigation is needed to clarify the climatic context and interactions between EASM and westerlies circulation during this period.

5. Conclusions

In summary, we have presented multiple biomarker records from the upwelling region of the northern SCS coast, which consistently document the strength of summer monsoon-induced upwelling and thus Holocene EASM variability. Our results show substantially enhanced EASM strength during ~6000–9000 cal a BP and ~3300–4500 cal a BP, superimposed on the long-term Holocene EASM weakening trend. The enhanced EASM strength during the Early to Middle Bronze Age challenges the presumed cool/dry climate background and offers a crucial climate context for the cultural developments and human evolution in East Asia. Our records, together with existing marine and terrestrial records, support a meridional tripole pattern of hydroclimatic variability over East Asia during the Early to Middle Bronze Age.

CRediT authorship contribution statement

Conceptualization: Z.L. Investigation: J.J., Z.L., Y.Z., H.L., H.W., Y.L., D.K., Z.X., H.Y., and W.L. Formal analysis: J.J., D.K., H.L., H.W., B.M., Y. L., W.M.L., and H.L. Funding acquisition: Z.L. Writing: J.J., Z.L., and Y.Z. led the writing with intellectual contributions from all coauthors.

Declaration of competing interest

The authors declare that they have no known competing financial interests or personal relationships that could have appeared to influence the work reported in this paper.

Acknowledgements

We thank the editor and two anonymous reviewers for their valuable comments and suggestions. This research was supported by National Key Research and Development Program of China (2023YFF0803901, to Z.L.) and Hong Kong Research Grants Council Grants (17316322, 17308424, to Z.L.).

Appendix A. Supplementary data

Supplementary data to this article can be found online at https://doi.org/10.1016/j.quascirev.2025.109439.

Data availability

All data is contained within the submission.

References

An, Z., Porter, S.C., Kutzbach, J.E., Wu, X., Wang, S., Liu, X., Li, X., Zhou, W., 2000. Asynchronous Holocene optimum of the East Asian monsoon. Quat. Sci. Rev. 19, 743–762.
Blaauw, M., Christen, J.A., 2011. Flexible paleoclimate age-depth models using an autoregressive gamma process. Bayesian Analysis 6, 457–474.
Blanco-González, A., Lillios, K.T., López-Sáez, J.A., Drake, B.L., 2018. Cultural, demographic and environmental dynamics of the Copper and Early Bronze Age in Iberia (3300–1500 BC): towards an interregional multiproxy comparison at the time of the 4.2 ky BP event. J. World PreHistory 31, 1–79.
Bond, G., Kromer, B., Beer, J., Muscheler, R., Evans, M.N., Showers, W., Hoffmann, S., Lotti-Bond, R., Hajdas, I., Bonani, G., 2001. Persistent solar influence on North Atlantic climate during the Holocene. Science 294, 2130–2136.
Cai, Y., Cheng, X., Ma, L., Mao, R., Breitenbach, S.F., Zhang, H., Xue, G., Cheng, H., Edwards, R.L., An, Z., 2021. Holocene variability of East Asian summer monsoon as viewed from the speleothem $\delta^{18}O$ records in central China. Earth Planet Sci. Lett. 558, 116758.
Cao, J., Chen, F., Chu, G., Jia, G., 2024. A persistent coast mode of precipitation in southeast China over the last millennium. Geophys. Res. Lett. 51, e2024GL109379.
Casey, K., 2013. US DOC/NOAA/NESDIS > National Oceanographic Data Center, AVHRR Pathfinder Version 5.0 Global 4km Sea Surface Temperature (SST) Cloud-Screened Monthly Climatologies for 1985-2006 (NODC Accession 0110657). National Oceanographic Data Center, NOAA, Version 1.1.
Chen, F.H., Dong, G.H., Zhang, D.J., Liu, X.Y., Jia, X., An, C.B., Ma, M.M., Xie, W.Y., Barton, L., Ren, X.Y., Zhao, Z.J., Wu, X.H., Jones, M.K., 2015. Agriculture facilitated permanent human occupation of the Tibetan Plateau after 3600 BP. Science 347, 248–250.
Chen, X., Deng, W., Xiao, H., Guo, H., Zeng, T., Zhao, J.X., Wei, G., 2023. Coral paleoclimate perspectives support the role of low-latitude forcing on the 4.2 ka BP event. Geophys. Res. Lett. 50, e2023GL104010.
Cheng, B., Chen, F., Zhang, J., 2013. Palaeovegetational and palaeoenvironmental changes since the last deglacial in Gonghe Basin, northeast Tibetan Plateau. J. Geogr. Sci. 23, 136–146.
Chiang, J.C.H., Swenson, L.M., Kong, W., 2017. Role of seasonal transitions and the westerlies in the interannual variability of the East Asian summer monsoon precipitation. Geophys. Res. Lett. 44, 3788–3795.
Davis, A.M., 1999. Quaternary stratigraphy of Hong Kong coastal sediments. J. Asian Earth Sci. 17, 521–531.
deMenocal, P.B., 2001. Cultural responses to climate change during the late Holocene. Science 292, 667–673.
Ding, Y., Wang, Z., Sun, Y., 2008. Inter-decadal variation of the summer precipitation in East China and its association with decreasing Asian summer monsoon. Part I: observed evidences. Int. J. Climatol. 28, 1139–1161.
Dykoski, C.A., Edwards, R.L., Cheng, H., Yuan, D., Cai, Y., Zhang, M., Lin, Y., Qing, J., An, Z., Revenaugh, J., 2005. A high-resolution, absolute-dated Holocene and deglacial Asian monsoon record from Dongge Cave, China. Earth Planet Sci. Lett. 233, 71–86.
Fyfe, J.A., Selby, I.C., Plater, A.J., Wright, M.R., 1999. Erosion and sedimentation associated with the last sea level rise offshore Hong Kong, South China Sea. Quat. Int. 55, 93–100.
Gupta, P., Gupta, A.K., Clemens, S.C., Cheng, H., Majhi, B., 2024. Coupled Ocean-Atmospheric forcing on Indian summer monsoon variability during the middle Holocene: insights from the core monsoon zone speleothem record. Palaeogeogr. Palaeoclimatol. Palaeoecol. 647, 112273.
Heaton, T.J., Köhler, P., Butzin, M., Bard, E., Reimer, R.W., Austin, W.E., Ramsey, C.B., Grootes, P.M., Hughen, K.A., Kromer, B., Reimer, P.J., Adkins, J., Burke, A., Cook, M. S., Olsen, J., Skinner, L.C., 2020. Marine20—the marine radiocarbon age calibration curve (0–55,000 cal BP). Radiocarbon 62, 779–820.
Hong, Y.T., Hong, B., Lin, Q.A., Shibata, Y., Hirota, M., Zhu, Y.X., Leng, X.T., Wang, Y., Wang, H., Yi, L., 2005. Inverse phase oscillations between the East Asian and Indian Ocean summer monsoons during the last 12000 years and paleo-El Niño. Earth Planet Sci. Lett. 231, 337–346.
Hosner, D., Wagner, M., Tarasov, P.E., Chen, X., Leipe, C., 2016. Spatiotemporal distribution patterns of archaeological sites in China during the Neolithic and Bronze Age: an overview. Holocene 26, 1576–1593.
Huang, X., Pancost, R.D., Xue, J., Gu, Y., Evershed, R.P., Xie, S., 2018. Response of carbon cycle to drier conditions in the mid-Holocene in central China. Nat. Commun. 9, 1369.
Huang, X., Zhang, H., Griffiths, M.L., Zhao, B., Pausata, F.S., Tabor, C., Shu, J., Xie, S., 2023. Holocene forcing of East Asian hydroclimate recorded in a subtropical peatland from southeastern China. Clim. Dyn. 60, 981–993.
Jia, G., Bai, Y., Yang, X., Xie, L., Wei, G., Ouyang, T., Chu, G., Liu, Z., Peng, P., 2015. Biogeochemical evidence of Holocene East Asian summer and winter monsoon variability from a tropical maar lake in southern China. Quat. Sci. Rev. 111, 51–61.
Jiang, J., Jiang, Y., Chan, M., Xin, Z., Xie, Z., Liu, Z., 2025. Summer monsoon-induced costal upwelling variability documented by sea surface temperature changes in the Min-Zhe mud area over the last two millennia. Quat. Sci. 45, 579–587.
Jiang, J., Meng, B., Wang, H., Liu, H., Song, M., He, Y., Zhao, C., Cheng, J., Chu, G., Krivonogov, S., Liu, W., Liu, Z., 2024. Spatial patterns of Holocene temperature changes over mid-latitude Eurasia. Nat. Commun. 15, 1507.
Jiang, Q., Meng, B., Wang, Z., Qian, P., Zheng, J., Jiang, J., Zhao, C., Hou, J., Dong, G., Shen, J., Liu, W., Liu, Z., Chen, F., 2022. Exceptional terrestrial warmth around 4200–2800 years ago in Northwest China. Sci. Bull. 67, 427–436.
Jiang, S., Zhou, X., Sachs, J.P., Luo, W., Tu, L., Liu, X., Zeng, L., Peng, S., Yan, Q., Liu, F., Zheng, J., Zhang, J., Shen, Y., 2021. Central eastern China hydrological changes and ENSO-like variability over the past 1800 yr. Geology 49, 1386–1390.
Jiang, W., Guo, Z., Sun, X., Wu, H., Chu, G., Yuan, B., Hatté, C., Guiot, J., 2006. Reconstruction of climate and vegetation changes of lake Bayanchagan (Inner Mongolia): Holocene variability of the East Asian monsoon. Quat. Res. 65, 411–420.
Kajita, H., Kawahata, H., Wang, K., Zheng, H., Yang, S., Ohkouchi, N., Utsunomiya, M., Zhou, B., Zheng, B., 2018. Extraordinary cold episodes during the mid-Holocene in the Yangtze delta: interruption of the earliest rice cultivating civilization. Quat. Sci. Rev. 201, 418–428.
Kathayat, G., Cheng, H., Sinha, A., Yi, L., Li, X., Zhang, H., Li, H., Ning, Y., Edwards, R.L., 2017. The Indian monsoon variability and civilization changes in the Indian subcontinent. Sci. Adv. 3, e1701296.
Kim, J.H., Van der Meer, J., Schouten, S., Helmke, P., Willmott, V., Sangiorgi, F., Koç, N., Hopmans, E.C., Sinninghe Damsté, J.S., 2010. New indices and calibrations derived from the distribution of crenarchaeal isoprenoid tetraether lipids: implications for past sea surface temperature reconstructions. Geochem. Cosmochim. Acta 74, 4639–4654.
Kong, D., Tse, Y.Y., Jia, G., Wei, G., Chen, M.T., Zong, Y., Liu, Z., 2015. Cooling trend over the past 4 centuries in northeastern Hong Kong waters as revealed by alkenone-derived SST records. J. Asian Earth Sci. 114, 497–503.
Kong, D., Zong, Y., Jia, G., Wei, G., Chen, M.T., Liu, Z., 2014. The development of late Holocene coastal cooling in the northern South China Sea. Quat. Int. 349, 300–307.
Laskar, J., Robutel, P., Joutel, F., Gastineau, M., Correia, A.C., Levrard, B., 2004. A long-term numerical solution for the insolation quantities of the Earth. Astron. Astrophys. 428, 261–285.

Lee, W.M., Poon, K.C., Kong, D., Sewell, R.J., Zong, Y., Zhang, Y., Liu, Z., 2019. Summer monsoon–induced upwelling dominated coastal sea surface temperature variations in the northern South China Sea over the last two millennia. Holocene 29, 691–698.
Li, C., Yu, S.Y., Yao, S., Shen, J., Ji, M., Chen, R., Sun, W., Ling, C., 2019. Response of alpine vegetation to climate changes in the Nanling Mountains during the second half of the Holocene. Quat. Int. 522, 12–22.
Li, J., Liu, X., 2018. Orbital- and suborbital-scale changes in the East Asian summer monsoon since the last deglaciation. Holocene 28, 1216e1224.
Li, Q., Wu, H., Cheng, J., Zhang, W., Yu, Y., Sun, A., Luo, Y., 2024. Hydroclimatic changes in eastern China during the Holocene based on pollen data and climate modeling. Global Planet. Change 234, 104391.
Lin, J., Jiang, W., Wang, L., Zhang, E., Tang, L., Yang, X., Chu, G., Yang, S., Xiao, J., 2022. Spatially diverse hydroclimatic response to the 4.2 ka event in the Asian monsoon region. Quat. Sci. Rev. 296, 107809.
Liu, J., Chen, J., Zhang, X., Li, Y., Rao, Z., Chen, F., 2015. Holocene East Asian summer monsoon records in northern China and their inconsistency with Chinese stalagmite $\delta^{18}O$ records. Earth Sci. Rev. 148, 194–208.
Liu, Z., Wen, X., Brady, E.C., Otto-Bliesner, B., Yu, G., Lu, H., Cheng, H., Wang, Y., Zheng, W., Ding, Y., Edwards, R.L., Cheng, J., Liu, W., Yang, H., 2014. Chinese cave records and the East Asia summer monsoon. Quat. Sci. Rev. 83, 115–128.
Locarnini, M.M., Mishonov, A.V., Baranova, O.K., Boyer, T.P., Zweng, M.M., Garcia, H.E., Reagan, J.R., Seidov, D., Weathers, K.W., Paver, C.R., Smolyar, I., 2018. World Ocean Atlas 2018, Volume 1: Temperature, vol. 81. NOAA Atlas NESDIS, p. 52.
Lu, F., Ma, C., Zhu, C., Lu, H., Zhang, X., Huang, K., Guo, T., Li, K., Li, L., Li, B., Zhang, W., 2019. Variability of East Asian summer monsoon precipitation during the Holocene and possible forcing mechanisms. Clim. Dyn. 52, 969–989.
Ma, T., Rolett, B.V., Zheng, Z., Zong, Y., 2020. Holocene coastal evolution preceded the expansion of paddy field rice farming. Proc. Natl. Acad. Sci. 117, 24138–24143.
Marcott, S.A., Shakun, J.D., Clark, P.U., Mix, A.C., 2013. A reconstruction of regional and global temperature for the past 11,300 years. Science 339, 1198–1201.
McKay, N.P., Kaufman, D.S., Arcusa, S.H., Kolus, H.R., Edge, D.C., Erb, M.P., Hancock, C. L., Routson, C.C., Żarczyński, M., Marshall, L.P., Roberts, G.K., Telles, F., 2024. The 4.2 ka event is not remarkable in the context of Holocene climate variability. Nat. Commun. 15, 6555.
Pelejero, C., Grimalt, J.O., 1997. The correlation between the U37K'index and sea surface temperatures in the warm boundary: the South China Sea. Geochem. Cosmochim. Acta 61, 4789–4797.
Prahl, F., Muehlhausen, L., Zahnle, D., 1988. Further evaluation of long-chain alkenones as indicators of paleoceanographic conditions. Geochem. Cosmochim. Acta 52, 2303–2310.
Railsback, L.B., Liang, F., Brook, G.A., Voarintsoa, N.R.G., Sletten, H.R., Marais, E., Hardt, B., Cheng, H., Edwards, R.L., 2018. The timing, two-pulsed nature, and variable climatic expression of the 4.2 ka event: a review and new high-resolution stalagmite data from Namibia. Quat. Sci. Rev. 186, 78–90.
Schouten, S., Hopmans, E.C., Schefuß, E., Damste, J.S.S., 2002. Distributional variations in marine crenarchaeotal membrane lipids: a new tool for reconstructing ancient sea water temperatures? Earth Planet Sci. Lett. 204, 265–274.
Stebich, M., Rehfeld, K., Schluetz, F., Tarasov, P.E., Liu, J., Mingram, J., 2015. Holocene vegetation and climate dynamics of NE China based on the pollen record from Sihailongwan Maar Lake. Quat. Sci. Rev. 124, 275–289.
Steinhilber, F., Abreu, J.A., Beer, J., Brunner, I., Christl, M., Fischer, H., Heikkilä, U., Kubik, P.W., Mann, M., McCracken, K.G., Miller, H., Miyahara, H., Oerter, H., Wilhelms, F., 2012. 9,400 years of cosmic radiation and solar activity from ice cores and tree rings. Proc. Natl. Acad. Sci. 109, 5967–5971.
Sun, Q., Liu, Y., Wünnemann, B., Peng, Y., Jiang, X., Deng, L., Chen, J., Li, M., Chen, Z., 2019. Climate as a factor for Neolithic cultural collapses approximately 4000 years BP in China. Earth Sci. Rev. 197, 102915.
Tan, L., Cai, Y., Cheng, H., Edwards, L.R., Gao, Y., Xu, H., Zhang, H., An, Z., 2018. Centennial-to decadal-scale monsoon precipitation variations in the upper Hanjiang River region, China over the past 6650 years. Earth Planet Sci. Lett. 482, 580–590.
Tierney, J.E., Tingley, M.P., 2018. BAYSPLINE: a new calibration for the alkenone paleothermometer. Paleoceanogr. Paleoclimatol. 33, 281–301.
Wang, H., Chen, J., Zhang, X., Chen, F., 2014. Palaeosol development in the Chinese Loess Plateau as an indicator of the strength of the East Asian summer monsoon: evidence for a mid-Holocene maximum. Quat. Int. 334, 155–164.
Wang, H., Liu, W., Lu, H., Zhang, Y., Liang, Y., He, Y., Bohaty, S.M., Wilson, P.A., Liu, Z., 2023a. Oxygenated deep waters fed early Atlantic overturning circulation upon Antarctic glaciation. Nat. Geosci. 16, 1014–1019.
Wang, M., Wang, H., Zhu, Z., Yang, X., Zhang, K., Zhang, Y., Liu, W., Zheng, Z., Zong, Y., Liu, Z., 2021. Late Miocene-Pliocene Asian summer monsoon variability linked to both tropical Pacific temperature and Walker Circulation. Earth Planet Sci. Lett. 561, 116823.
Wang, M., Xiong, H., Yang, S., Yu, F., Kong, D., Zong, Y., Liu, Z., 2023b. Assessing the U37K'-sea surface temperature relationship in shallow marine waters. Sci. China Earth Sci. 66, 918–928.
Wang, Y., Cheng, H., Edwards, R.L., He, Y., Kong, X., An, Z., Wu, J., Kelly, M.J., Dykoski, C.A., Li, X., 2005. The Holocene Asian monsoon: links to solar changes and North Atlantic climate. Science 308, 854–857.
Wu, J., Liu, Q., Cui, Q.Y., Xu, D.K., Wang, L., Shen, C.M., Chu, G.Q., Liu, J.Q., 2019. Shrinkage of East Asia winter monsoon associated with increased ENSO events since the mid-Holocene. J. Geophys. Res. Atmos. 124, 3839–3848.
Xiang, L., Huang, X., Zhang, J., Huang, C., Schwalb, A., Zhang, J., Rudaya, N., Sun, M., Mu, X., Li, Y., Luo, D., Muhuammad, F., Zhang, W., Wang, W., Wang, T., Zheng, M., Ren, X., Zhang, J., Zhang, E., Gou, X., Chen, F., 2024. First Pediastrum–temperature transfer function and its application to mid-to-late Holocene reconstruction in Central Asia. Quat. Sci. Rev. 327, 108516.
Xiao, J., Xu, Q., Nakamura, T., Yang, X., Liang, W., Inouchi, Y., 2004. Holocene vegetation variation in the Daihai Lake region of north-central China: a direct indication of the Asian monsoon climatic history. Quat. Sci. Rev. 23, 1669–1679.
Xie, S., Evershed, R.P., Huang, X., Zhu, Z., Pancost, R.D., Meyers, P.A., Gong, L., Hu, C., Huang, J., Zhang, S., Gu, Y., Zhu, J., 2013. Concordant monsoon-driven postglacial hydrological changes in peat and stalagmite records and their impacts on prehistoric cultures in central China. Geology 41, 827–830.
Xing, L., Sachs, J., Gao, W., Tao, S., Zhao, X., Li, L., Liu, Y., Zhao, M., 2015. TEX_{86} palaeothermometer as an indication of bottom water temperature in the Yellow Sea. Org. Geochem. 86, 19–31.
Xu, H., Song, Y., Cao, J., Lan, J., Zhang, J., Zhou, K.E., Wang, J., Cheng, O.P., Hong, B., Cheng, J., Tan, L., 2024. Heterogeneity of the East Asian rainfall influenced by solar-forced western Pacific subtropical high. Commun. Earth Environ. 5, 521.
Yang, X., Yang, H., Wang, B., Huang, L.J., Shen, C.C., Edwards, R.L., Cheng, H., 2019. Early-Holocene monsoon instability and climatic optimum recorded by Chinese stalagmites. Holocene 29, 1059–1067.
Yu, S.Y., Hou, Z., Chen, X., Wang, Y., Song, Y., Gao, M., Pan, J., Sun, M., Fang, H., Han, J., Kidder, T.R., Chen, F.H., 2020. Extreme flooding of the lower Yellow River near the Northgrippian-Meghalayan boundary: evidence from the Shilipu archaeological site in southwestern Shandong Province, China. Geomorphology 350, 106878.
Zhang, H., Cheng, H., Sinha, A., Spötl, C., Cai, Y., Liu, B., Kathayat, G., Li, H., Tian, Y., Li, Y., Zhao, J., Sha, L., Lu, J., Meng, B., Niu, X., Dong, X., Liang, Z., Zong, B., Ning, Y., Lan, J., Edwards, R.L., 2021a. Collapse of the Liangzhu and other Neolithic cultures in the lower Yangtze region in response to climate change. Sci. Adv. 7, eabi9275.
Zhang, H., Griffiths, M.L., Chiang, J.C., Kong, W., Wu, S., Atwood, A., Huang, J., Cheng, H., Ning, Y., Xie, S., 2018. East Asian hydroclimate modulated by the position of the westerlies during Termination I. Science 362, 580–583.
Zhang, Y., Zheng, X., Kong, D., Yan, H., Liu, Z., 2021b. Enhanced North Pacific subtropical gyre circulation during the late Holocene. Nat. Commun. 12, 5957.
Zhang, Y., Zhu, K., Huang, C., Kong, D., He, Y., Wang, H., Liu, W., Xie, Z., Wei, G., Liu, Z., 2019. Asian winter monsoon imprint on Holocene SST changes at the northern coast of the South China Sea. Geophys. Res. Lett. 46, 13363–13370.
Zhang, Y., Zhu, K., Huang, C., Kong, D., He, Y., Wang, H., Liu, W., Xie, Z., Wei, G., Liu, Z., 2021c. Asian winter monsoon imprint on the water column structure at the northern South China Sea coast. Front. Earth Sci. 9, 680180.
Zhao, K., Wang, Y., Edwards, R.L., Cheng, H., Liu, D., Kong, X., Ning, Y., 2016. Contribution of ENSO variability to the East Asian summer monsoon in the late Holocene. Palaeogeogr. Palaeoclimatol. Palaeoecol. 449, 510–519.
Zhao, L., Zeng, Y., Rao, Z., Huang, C., Li, Y., Liu, L., Ma, C., 2024. Quantitative Holocene climate reconstruction and anthropogenic impact analysis based on the pollen records in peat sediment in Southern China. Global Planet. Change 234, 104390.
Zhong, W., Cao, J., Xue, J., Ouyang, J., 2015. A 15,400-year record of climate variation from a subalpine lacustrine sedimentary sequence in the western Nanling Mountains in South China. Quat. Res. 84, 246–254.
Zhong, W., Xue, J., Zheng, Y., Ouyang, J., Ma, Q., Cai, Y., Tang, X., 2010. Climatic changes since the last deglaciation inferred from a lacustrine sedimentary sequence in the eastern Nanling Mountains, south China. J. Quat. Sci. 25, 975–984.
Zhou, X., Sun, L., Zhan, T., Huang, W., Zhou, X., Hao, Q., Wang, Y., He, X., Zhao, C., Qiao, Y., Ge, J., Yan, P., Shao, D., Chu, Z., Yang, W., Smol, J.P., 2016. Time-transgressive onset of the Holocene optimum in the East Asian monsoon region. Earth Planet Sci. Lett. 456, 39–46.
Zweng, M., Reagan, J., Seidov, D., Boyer, T., Locarnini, M., Garcia, H., Mishonov, A., Baranova, O., Weathers, K., Paver, C., Smolyar, I., 2019. World Ocean Atlas 2018, Volume 2: Salinity, vol. 82. NOAA Atlas NESDIS, p. 50.